Catalysis Science & Technology

www.rsc.org/catalysis

Volume 1 | Number 1 | Jan 2013 | Pages 1–100

ROYAL SOCIETY OF CHEMISTRY

www.rsc.org/catalysis

Journal Name

ARTICLE

Effect of preparation method on the solid state properties and the deN$_2$O performance of CuO-CeO$_2$ oxides

M. Konsolakis[a*], S.A.C. Carabineiro[b], E. Papista[c], G.E. Marnellos[c,d], P.B. Tavares[e], J. Agostinho Moreira[f], Y. Romaguera-Barcelay[f], J.L. Figueiredo[e]

The present work aims at investigating the catalytic decomposition of N$_2$O over CuO-CeO$_2$ single or mixed oxides prepared by different synthesis routes, i.e., impregnation, precipitation and exotemplating. To gain insight into the particular role of CeO$_2$ as well as of CuO-CeO$_2$ interactions, three different types of materials are prepared and tested for N$_2$O decomposition both in the absence and presence of excess O$_2$: (i) bare CeO$_2$ prepared by precipitation and exotemplating, (ii) CuO/CeO$_2$ oxides synthesized by impregnation of CeO$_2$ samples prepared in (i) with CuO and iii) single stage synthesized CuO-CeO$_2$ mixed oxides employing the co-precipitation and exotemplating methods. The corresponding commercial samples were also examined for comparison purposes. All materials were characterized by N$_2$ adsorption at -196 °C, X-ray diffraction (XRD), H$_2$ temperature-programmed reduction (H$_2$-TPR), X-ray photoelectron spectroscopy (XPS), micro-Raman spectroscopy (micro-Raman) and scanning electron microscopy (SEM). The results demonstrated the key role of preparation procedure on the direct catalytic decomposition of N$_2$O. Among the bare CeO$_2$ samples, the best performance was obtained with the samples prepared by the precipitation method, followed by exotemplating, while commercial CeO$_2$ showed the lowest performance. All bare oxides demonstrated low N$_2$O conversion, never exceeding 40% at 600 °C. Amongst the CuO-CeO$_2$ oxides, the optimum performance was observed for those prepared by co-precipitation, which achieved complete N$_2$O conversion at 550 ºC. In the presence of excess oxygen in the feed stream, a slight degradation is observed, with the sequence of deN$_2$O performance to remain unchanged. The superiority of Cu-Ce mixed oxides prepared by precipitation compared to all other materials can be mainly ascribed to their excellent redox properties, linked to Ce^{4+}/Ce^{3+} and Cu^{2+}/Cu$^+$ redox pairs. A redox mechanism for N$_2$O catalytic decomposition is proposed involving N$_2$O adsorption on Cu$^+$ sites and their regeneration through Cu-ceria interactions.

[a]*School of Production Engineering and Management, Technical University of Crete, 73100 Chania, Greece.*
E-mail: mkonsol@science.tuc.gr; Tel: +30 28210 37682;
Web: www.tuc.gr/konsolakis.html (M. Konsolakis)
[b]*Laboratório de Catálise e Materiais (LCM), Laboratório Associado LSRE/LCM, Faculdade de Engenharia, Universidade do Porto, 4200-465 Porto, Portugal*
[c]*Department of Mechanical Engineering, University of Western Macedonia, GR-50100 Kozani, Greece*
[d]*Chemical Process & Energy Resources Institute, Centre for Research & Technology Hellas, GR-57001, Thessaloniki, Greece*
[e]*CQVR Centro de Química–Vila Real, Dep.Química, Universidade de Trás-os-Montes e Alto Douro, 5001-911 Vila Real, Portugal*
[f]*IFIMUP and IN-Inst. Nanoscience and Nanotechnology, Departamento de Física e Astronomia da Faculdade de Ciências, Universidade do Porto, 4169-007 Porto, Portugal*

Introduction

Nitrous oxide (N$_2$O) is recognized as one of the six most powerful greenhouse gases, with a high global warming potential (around 300 times higher compared to CO$_2$) and a long lifetime in atmosphere (almost 150 years), that severely contributes to the destruction of stratospheric ozone layer[1,2]. According to recent studies, the ozone depleting potential of N$_2$O is comparable to that of hydrochlorofluorocarbons (HCFCs), which are known as the most important ozone depleting agents[3]. Although N$_2$O is emitted by both natural and anthropogenic sources, the significant annual increase of its concentration in the atmosphere is mainly attributed to human activities, such as adipic and nitric acid plants, fuel combustion processes, etc[4,5]. Therefore, the effective control of N$_2$O stationary

and mobile emissions is nowadays a challenging environmental issue.

Several after-treatment techniques have been developed for N_2O abatement, including thermal decomposition[6], non-selective catalytic reduction[4], selective catalytic reduction[7,8] and direct catalytic decomposition[9-12]. Among these, direct catalytic decomposition of N_2O (deN_2O) is the most promising method, due to its high efficiency and low energy requirements. The decomposition of N_2O has been studied on various catalytic systems, such as transition and noble metal catalysts, perovskites, hexaluminates, spinels, zeolites, etc[4,9,13-20]. In spite of the excellent catalytic performance of noble metals (NMs)-based catalysts, their high cost and sensitivity to oxygen poisoning limit their practical applications[9]. Therefore, the development of NMs-free catalysts of low cost and adequate de-N_2O performance is of crucial importance from both practical and economical point of view[4].

Recently, it has been reported that mixed oxides could be possible alternatives for N_2O catalytic decomposition[20,21]. In most of these studies, CeO_2 is used as a basic component in mixed oxides, due to its unique physicochemical properties linked to high oxygen storage-release capacity *via* Ce^{4+}/Ce^{3+} redox cycles[22]. In this regard, several CeO_2-based mixed oxides, such as Fe_2O_3-CeO_2[20], Co_3O_4-CeO_2[21], CuO-Co_3O_4[23], CuO-CeO_2[24-27], were tested for N_2O decomposition. An enhanced performance of mixed oxides compared to individual counterparts is usually obtained, which is ascribed to better redox properties through synergistic metal-support interactions.

Lately, Cu-based catalysts have also received considerable attention in heterogeneous catalysis due to their adequate performance and low cost[28]. Cu-based catalysts have shown great potential as alternatives to NMs for several applications such as oxidation of volatile organic compounds (VOCs), water-gas-shift (WGS) reaction, CO oxidation, preferential oxidation (PROX), steam reforming, among others[29-34].

In the line of the above aspects, it has been clearly verified that CuO-CeO_2 oxides confer a synergistic interaction effect toward enhanced reducibility and catalytic performance[35-40]. The intrinsic reactivity of mixed oxides counterparts (e.g. CuO, CeO_2, Co_3O_4, etc) is very important, but the synthesis procedure is also expected to have a critical role on the interactions between oxides and consequently on the redox properties and catalytic performance. Adamski *et al.*[25], investigated the impact of preparation method of Cu/CeO_2 catalysts

on deN_2O performance. It was reported that 5 mol% Cu/CeO_2 sample prepared by impregnation demonstrated the best deN_2O performance. Zhou *et al.*[26] found that 67 mol% Cu/CeO_2 catalyst prepared by citrate method provided the highest N_2O conversion. Zabilski *et al.*[27] studied the N_2O decomposition in a series of Cu/CeO_2 samples with different Cu content, prepared by applying a hard template replication approach, using silica KIT-6 as template. They showed that Cu loadings in the range of 20-40 mol% resulted in the optimum deN_2O performance. A close correlation between catalytic activity and reducibility was revealed[27].

Taking into account the unique properties of CuO-CeO_2 mixed oxides, as well as the critical role of synthesis procedure on their solid state properties, the present work aims at systematically exploring the catalytic decomposition of N_2O over CuO-CeO_2 single or mixed oxides prepared by different routes, *i.e.*, impregnation, precipitation and exotemplating. To gain insight into the particular role of CeO_2 properties as well as on CuO-CeO_2 interactions three different types of materials are prepared and tested for N_2O decomposition both in the absence and presence of O_2 excess: (i) bare CeO_2 prepared by precipitation and exotemplating, in comparison to commercial CeO_2, (ii) CuO/CeO_2 mixed oxides synthesized by impregnation of CeO_2 samples prepared in (i) with CuO and iii) CuO-CeO_2 mixed oxides prepared at one stage through impregnation, co-precipitation and exotemplating. Several characterizations techniques (BET, XRD, SEM, TPR, micro-Raman and XPS) were employed to reveal the influence of synthesis procedure on the physicochemical properties of the prepared samples and their impact on N_2O decomposition.

Experimental

Materials Synthesis

Preparation of bare CeO_2

CeO_2 was synthesized by two different methods: precipitation and exotemplating. The first method is consisting in adding 0.5 M NaOH solution to 0.5 M of cerium nitrate solution ($Ce(NO_3)_3 \cdot 6H_2O$) with stirring, until pH= 8[41,42]. The resulting precipitate was aged at room temperature overnight, filtered, washed with distilled water and dried at 100 ℃. Then the samples were calcined for 5 h at 600 ℃ (100 cm^3/min air flow) with a heating rate of 2 ℃/min. Ce-pp samples was obtained by this route.

Exotemplating was based on the procedure proposed by Schwickardi *et al.*[43], which was similar to that used in other works[41,42,44-49]. A carbon xerogel prepared by condensation of resorcinol and formaldehyde at pH= 6, following the method described in previous works[50-53], was used as template. Its BET surface area was 650 m^2/g and the mesopore size equaled to 25 nm. Particle sizes between 0.05 and 0.25 mm were used. A saturated solution of a cerium nitrate precursor (Sigma-Aldrich) was added to the template by impregnation. Excess precursor solution was then removed by vacuum filtration and residual liquid on the surface of the template material was removed by sandwiching the solid phase between two sheets of filter paper and squeezing gently. Then the impregnated template material was dried in an oven overnight at 100 ℃ and calcined for 5 h at 600 ℃ in air (100 cm^3/min). Total carbon template removal was achieved and the Ce-exo sample was obtained. A commercial ceria (Fluka) was also used for comparison purposes (Ce-com sample). This sample was calcined at the same conditions as the other samples.

Preparation of CuO/ceria samples

The ceria materials obtained above were impregnated in an aqueous solution of $Cu(NO_3)_2 \cdot 6H_2O$ (Sigma Aldrich) with appropriate concentration, so as to yield 20 wt.% Cu loading[29]. The resulting suspension was heated under stirring until water evaporation, dried at 120 ℃ overnight and calcined at 600 ℃ for 5 h at the same conditions as the ceria materials. Following the aforementioned procedure the Ce-pp+Cu, Ce-exo+Cu and Ce-com+Cu materials were synthesized.

Preparation of Ce-Cu mixed oxides

Ce-Cu mixed oxides with 20 wt.% Cu loading were prepared by using cerium and copper nitrates (Sigma Aldrich) as precursors[54]. Samples were prepared by precipitation and exotemplating, following the procedure described above for the ceria materials. Briefly, during the precipitation method, NaOH was added to the mixture of Ce and Cu nitrate precursors of appropriate concentration, in order to obtain 20 wt.% Cu loading. The resulting suspension was aged at room temperature overnight, filtrated, washed, dried at 100 ℃ and calcined at 600 ℃ for 5 h. Ce-Cu-pp samples were obtained by this route.

For the preparation of Ce-Cu mixed oxides by exotemplating, the carbon xerogel template was co-impregnated with a mixture of saturated solutions of Ce and Cu nitrate precursors, in order to obtain

catalysts with 20 wt.% Cu. The excess solution was removed by vacuum filtration; the residual liquid was eliminated by sandwiching the solid phase between two sheets of filter paper with squeezing gently, followed by drying overnight at 100 ℃ and calcination at 600 ℃ for 5 h. Ce-Cu-exo materials were obtained.

For comparison, commercial CeO_2 (Fluka) and commercial CuO (Riedel-de Haën) were mechanically mixed in order to obtain Ce-Cu oxide with 20 wt.% Cu loading (Ce-Cu-com). The mixture was calcined at 600 ℃ for 5 h, as followed for the mixed oxides prepared by precipitation and exotemplating.

For all samples the Cu loading was kept constant at 20 wt.%, corresponding on atomic basis to ~18 at%. This specific loading was selected taking into account the sufficient catalytic performance of Cu/CeO_2 samples with a Cu loading in the range of 10-20 at%[27,29,31,54,55]. Furthermore, in relevant studies, it was clearly revealed that a Cu content of 10-20 at% results in the formation of easily reduced small copper clusters, while for loadings higher than 40 at% copper is present mainly as large CuO particles, which do not interact strongly with the support[56].

Materials Characterization

The prepared metal oxides were characterized by N_2 adsorption at -196 ℃, scanning electron microscopy/energy-dispersive X-ray spectroscopy (SEM/EDS), X-ray diffraction (XRD), temperature programmed reduction (TPR), micro-Raman spectroscopy (micro-Raman) and X-ray photoelectron spectroscopy (XPS). TG-DSC was carried out in a Netzsch STA 409 PC Luxx1 apparatus for the exotemplated materials. The mass used for each test was around 15 mg. This amount of sample was weighed and placed in a ceramic crucible. Experiments were carried out in air with a heating rate of 10 ℃/min until 800 ℃. This technique allowed checking the presence of residual carbon template in the samples after calcination.

Textural characterization (BET)

The textural characterization was obtained from the N_2 adsorption isotherms measured in a Quantachrome Instruments Nova 4200e apparatus. All samples were previously degassed at 160 ℃ for 5 h before analysis. The specific surface area (S_{BET}) was calculated by the Brunauer–Emmett–Teller (BET) equation[57].

Structural characterization (XRD)

XRD analysis was carried out in a PAN'alytical X'Pert MPD equipped with a X'Celerator detector and a secondary

monochromator (Cu Kα = 0.154 nm, 50 kV, 40 mA). The collected spectra were analysed by Rietveld refinement using PowderCell software, allowing the determination of crystallite sizes.

Morphological characterization (SEM)

Surface analysis for morphological characterisation was carried out by SEM, using a FEI Quanta 400 FEG ESEM (15 keV) electron microscope. The sample powders were mounted on a double-sided adhesive tape and observed at different magnifications under two different detection modes, secondary and back-scattered electrons. EDXS confirmed the nature of the components.

Redox characterization (TPR)

TPR experiments were carried out in a fully automated AMI-200 Catalyst Characterization Instrument (Altamira Instruments) under H_2 atmosphere, to acquire information on the reducibility of the samples. In a typical TPR experiment, 50 mg of sample was placed in a U-shaped quartz tube located inside an electrical furnace and heated to 100 ºC at 10 ºC/min under He flow of 29 cm^3/min and H_2 flow of 1.5 cm^3/min.

Surface characterization (XPS)

The XPS analysis was performed using a Kratos AXIS Ultra HSA, with VISION software for data acquisition and CASAXPS software for data analysis. The analysis was carried out with a monochromatic Al Kα X-ray source (1486.7 eV), operating at 15kV (90 W), in FAT mode (Fixed Analyser Transmission), with a pass energy of 40 eV for regions ROI and 80 eV for survey. Data acquisition was performed with a pressure lower than 1×10^{-6} Pa, and it was used a charge neutralisation system. The effect of the electric charge was corrected by the reference of the carbon peak (285 eV).

Structural/surface characterization (micro-Raman)

Unpolarized micro-Raman spectra were recorded at room conditions using a LamRam Jobin Yvon spectrometer and the 532 nm laser line as excitation. The spectral resolution was about 2 cm^{-1}. The laser power was kept at 10 mW in order to avoid sample heating.

Catalytic activity measurements

Catalytic activity experiments were performed in a cylindrical, quartz U-shaped fixed-bed reactor, with an inner diameter of 8 mm. The reactor loading was 100 mg, diluted with an equal amount of quartz. The total gas flow rate was 150 cm^3 (STP)/min corresponding to a Gas Hourly Space Velocity (GHSV) of 40000 h^{-1}. The feed

composition during N_2O catalytic decomposition experiments was 1000 ppm N_2O or 1000 ppm N_2O + 2.0 v/v% O_2, balanced with He. The N_2O conversion performance was monitored in the temperature range of 200 to 600 ºC. Effluents' composition was analyzed by a gas chromatograph (Shimadzu 14B) equipped with a thermal conductivity detector (TCD) and a combination of Porapak QS and Molecular Sieve 5A columns.

Results and discussion

Textural characterization

The textural properties of the materials are listed in Table 1. Among the bare CeO_2 samples, the superior textural characteristics, in terms of surface area, of Ce-pp (68 m^2/g) and Ce-exo (42 m^2/g) samples compared to Ce-com (15 m^2/g), is revealed, in accordance to previous studies[54]. Addition of Cu to ceria by impregnation results in a decrease of the surface area, due to the blockage of support porous structure by CuO. The latter can be mainly ascribed to the relatively large crystallite size of CuO compared to CeO_2, as revealed by XRD (Table 1). In relation to Ce-Cu mixed oxides, exotemplate method results in a high surface area (119 m^2/g), which is double to that achieved with the precipitation method (57 m^2/g). The materials prepared by mechanically mixing commercial ceria and copper (Cu-Ce-com) have very low surface area (9 m^2/g), which is lying in values expected for a physical mixture.

Structural characterization (XRD)

Figure 1 depicts the XRD patterns of all samples. In Table 1 the main phases detected along with their crystallite sizes are presented. In all samples the presence of cerianite CeO_2 is confirmed (Figure 1 and Table 1). In samples containing both ceria and copper, CeO_2 cerianite along with CuO tenorite phases were identified. Among the bare ceria samples, Ce-com had the larger crystallite size (~54 nm), while those prepared in the lab (Ce-pp and Ce-exo) demonstrated a significantly lower size (around 16 nm). The latter is in accordance with the higher surface area of Ce-pp and Ce-exo samples, compared to Ce-com (Table 1). In Cu/CeO_2 samples prepared by the impregnation of copper phase on the differently prepared ceria precursors (Ce-pp+Cu, Ce-exo+Cu, Ce-com+Cu), the crystallite size of CeO_2 slightly changed compared to that of the corresponding bare CeO_2. The smallest CeO_2 crystallites (11.8 nm) were found for co-precipitated Ce-Cu-pp sample, which showed however the largest CuO particle size (43.7 nm). The size of CuO seems, in general, to follow an opposite trend to that of CeO_2.

Table 1. Summary of textural (BET), structural/surface (XRD, XPS, micro-Raman) and redox (TPR) characteristics of the prepared samples.

Samples	S_{BET} (m²/g)	Phase detected	Crystallite size (nm)	TPR peaks (°C)[a]	H₂ consumption (mmol g⁻¹)[b]	H₂ excess (mmol g⁻¹)[c]	Ce (III) %[d]	Cu(I) %[d]	Raman peaks[e] (cm⁻¹)
Ce-pp	68	CeO₂ cerianite	15.3	**277**, 493, 776	-	-	32	-	471
Ce-exo	42	CeO₂ cerianite	16.9	**279**, 495, 773	-	-	39	-	471
Ce-com	15	CeO₂ cerianite	54.2	**377**, 492, 764	-	-	36	-	471
Cu-com	6	CuO tenorite	35	**171**, *230*, 320	12.1	-	-	0	-
Ce-pp+Cu	36	CeO₂ cerianite CuO tenorite	15.5 40.1	**175**, 210, *227*, 752	3.25	0.83	28	3	456
Ce-exo+Cu	29	CeO₂ cerianite CuO tenorite	20.0 35.2	**167**, 206, *233*, 722	3.50	1.08	19	5	462
Ce-com+Cu	10	CeO₂ cerianite CuO tenorite	37.3 33.3	**215**, *232*, 271, 765	2.89	0.47	30	0	468
Ce-Cu-pp	57	CeO₂ cerianite CuO tenorite	11.8 43.7	**136**, 157, *197*, 750	3.45	1.03	45	12	448
Ce-Cu-exo	119	CeO₂ cerianite CuO tenorite	33.3 36.3	**141**, 159, *224*, 721	3.05	0.63	25	7	460
Ce-Cu-com	9	CeO₂ cerianite CuO tenorite	41.7 36.0	**160**, 185, *246*, 297, 765	3.52	1.10	31	0	456

[a]*TPR onset (bold), shoulders (italic) and peak maxima (plain text) temperatures*

[b]*estimated by the quantification of H₂ uptake in the low temperature range (100-400 °C) of TPR profiles*

[c]*estimated by the subtraction of H₂ required for CuO reduction in 20 wt.% Cu/CeO₂ samples (2.42 mmol g⁻¹) from the total H₂ consumption*

[d]*estimated by Cu2p and Ce3d XPS spectra*

[e]*F_{2g} mode of the cubic fluorite cerianite structure*
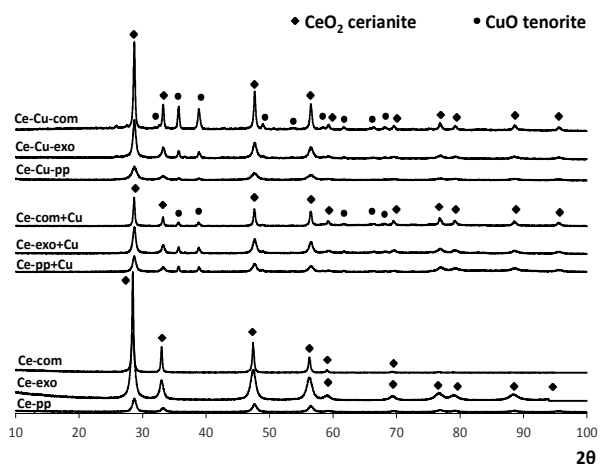
Figure 1. XRD diffractograms of ceria only and Ce-Cu mixed oxide samples.

Reducibility studies (H₂-TPR)

Figure 2 and Table 1 show the TPR results of the Ce containing samples. Figure 2a shows the TPR profiles of bare ceria samples. The TPR curves of Ce-pp and Ce-exo are very similar, characterized by two broad bands, while sharper peaks are obtained for Ce-com. Two characteristic peaks are observed: the peak centered at around 500 °C, corresponding to the reduction of surface oxygen (or reduction of surface oxygen species) and the peak at ~780 °C, related to the bulk oxygen[29,42,45,47,49].
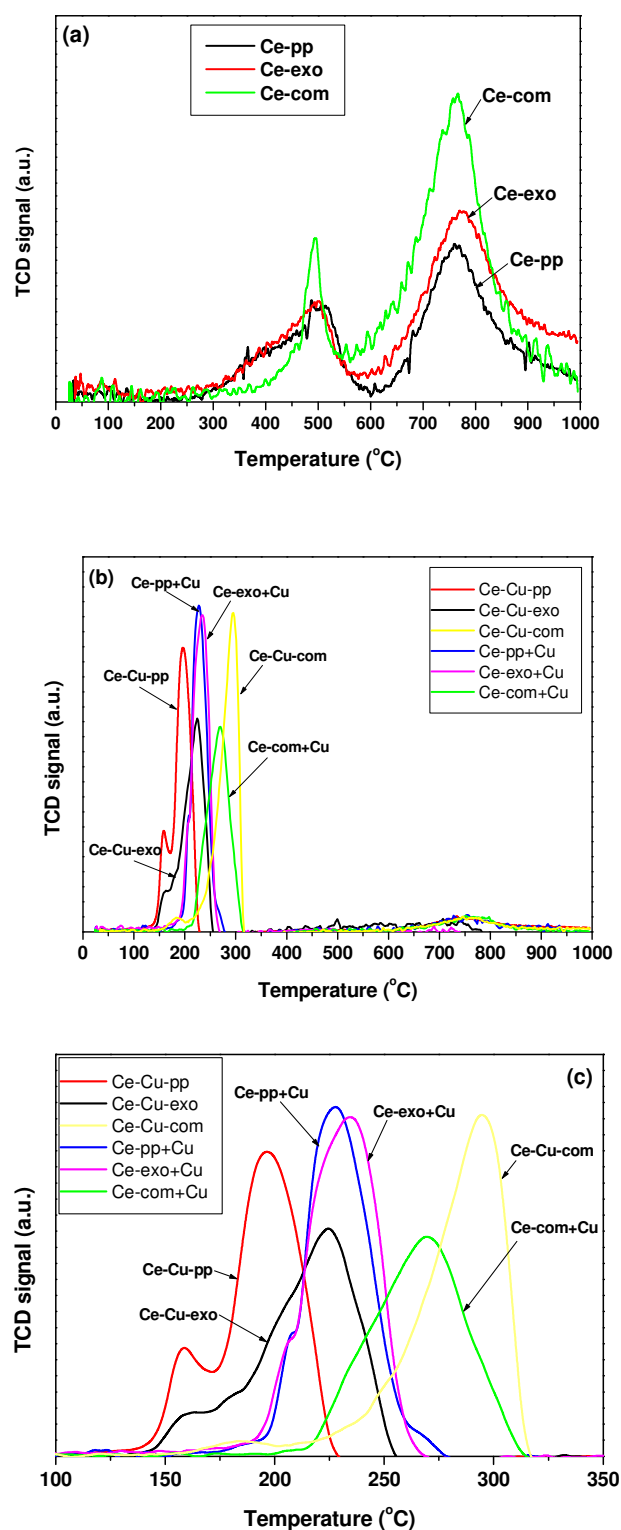
Figure 2. TPR profiles of ceria only samples (a) and Ce-Cu mixed oxide samples (b) with a closer detail at lower temperatures (c).

Figure 2b shows the TPR profiles of Cu-Ce samples. It is obvious that when Cu is added to CeO_2, the surface oxygen shell reduction is facilitated, resulting in a downward shift of TPR profiles[29]. This

indicates that the presence of Cu improves the reducibility of the surface oxygen on CeO_2 which, in turn, facilitates oxygen transfer across the solid–gas interface during reaction[29]. It is known that Cu oxide can show two reduction peaks (a main peak and a peak shoulder), around 150-300 ºC, which correspond to the CuO → Cu_2O and Cu_2O → Cu transitions[29,58], as seen in Table 1. Therefore, the peaks shown in the spectra of Ce-Cu samples (Figure 1c) are due to the improved reduction of surface oxygen of ceria, together with the reduction of CuO.

Interestingly, the mixed Ce-Cu oxides are more easily reducible than the Ce oxide materials impregnated with Cu, since their reduction peaks appear at lower temperatures (Table 1 and Figure 1c). Ce-Cu materials prepared by precipitation show better redox properties compared to those prepared by exotemplating. As expected, the materials prepared using commercial ceria and CuO exhibit the worst behavior, being the most difficult to be reduced.

Moreover, it is worth noting that Ce-Cu-pp samples, and to a lesser extent also Ce-Cu-exo samples, display a low temperature (LT) peak at ca. 160 ºC, which is usually ascribed to the reduction of finely dispersed CuO species closely interacting with CeO_2[27,59]. These species have been found to be very active for CO oxidation[59]. Interestingly, Ce-Cu-pp catalysts exhibited the optimum deN_2O performance (see below), implying a possible correlation between the low temperature reducibility and the catalytic performance, as will be discussed later.

To further gain insight into the impact of the preparation procedure on the redox properties of as prepared samples, the H_2 consumption in the low temperature range of TPR profiles (100-400 ºC, Figure 2), which corresponds to the surface oxygen reduction of copper and ceria species, is estimated. Results are shown in Table 1. By comparing the actual with the theoretical amount of H_2 consumption in bare CuO (Table 1), it is evident that the real H_2 uptake is very close to the theoretical one, implying a nearly complete reduction of CuO to Cu^0. However, the amount of H_2 required for the reduction of Cu-CeO_2 mixed oxides is always higher compared to that required for the complete reduction of CuO (2.42 mmol/g based on the nominal Cu loading of 20 wt.%). This "extra H_2", related mainly to ceria reduction, varies between 0.47 to 1.1 mmol H_2/g depending on the preparation procedure (Table 1). However, no obvious correlation between the H_2 amount related to ceria reduction and the preparation procedure is obtained (Table 1).

The superior reducibility of mixed oxides compared to single oxides can be mainly interpreted in terms of the strong interaction between copper and ceria, which in turn facilitates the reduction of CeO_2. In particular, the reduction of CeO_2 *via* the redox equilibrium: $Cu^{2+} + Ce^{3+} \rightarrow Cu^+ + Ce^{4+}$ can be considered responsible for the enhanced reducibility of Cu/CeO_2 samples, in terms of H_2 consumption, compared to bare oxides. More specifically, the superior reducibility of Cu/CeO_2 samples can be interpreted by taking into account two apparently alternative explanations: i) hydrogen spillover from Cu to the surface of ceria; dissociation of molecular hydrogen on Cu surface results in highly mobile atomic hydrogen which then reduces ceria by subtracting O^{2-} from its surface; ii) electronic metal support interactions (EMSI) between Cu and CeO_2. In the last case, the metal perturbs the electronic band structure of metal oxide, which is reduced directly by gas-phase H_2[60]. In this regard, a correlation has been established between the reduction temperature of ceria and the work function of the metal[61]. In a similar manner, a "junction effect theory" had been proposed earlier by Frost[62] in order to explain the mechanism by which noble metals electronically promote the redox characteristics of n-type metal oxides.

Surface morphology (SEM)

Samples were also analyzed by SEM. Figure 3 shows that Ce-pp has a "cotton-like" appearance (Figure 3a) and Ce-exo is more porous (Figure 3b), while Ce-com ceria has some nice flower-like features (Figure 3c), being more compact with some "holes".

Addition of Cu to these materials by impregnation did not result in significant changes in their morphology (Figures 3d-f). However some darker and lighter zones are observed (not shown in Figure 3, since the same amplification is shown for all samples), which are similar to those observed in Figure 3i (Ce-com+Cu-com). EDS reveals that the darker zones are Cu-rich areas (Figure 3l), while the lighter are Ce-rich areas (Figure 3k). On the other hand, Ce-Cu-pp (Fig. 3g) and Ce-Cu-exo (Fig. 3h) are uniform, without lighter/darker zones. The latter is ascribed to the uniform distribution of Ce and Cu, achieved when employing the co-precipitation and exotemplating methods, as the corresponding EDS reveals.
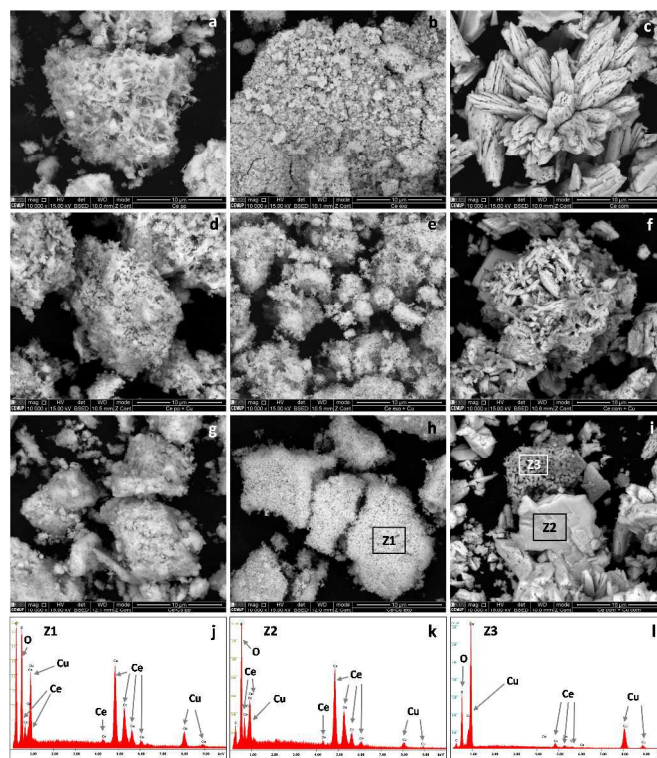
Figure 3. SEM images of Ce-pp (a), Ce-exo (b) Ce-com (c), Ce-pp+Cu (d), Ce-exo+Cu (e) Ce-com+Cu (f), Ce-Cu-pp (g), Ce-Cu-exo (h), Ce-Cu-com (i), and EDS spectra of zones marked as Z1 (j), Z2 (k) and Z3 (l).

Surface/structural characterization (XPS & micro-Raman)

To obtain information about the elemental chemical states and the surface composition, XPS measurements were performed. Figure 4 shows Ce 3d XPS results for all samples. The theoretical basis for all the components has been reported in the literature[42,63-67]. The complex spectra can be resolved into eight components by deconvolution with the assignment of each component defined in the figure (v represent the Ce $3d_{5/2}$ contributions and u represent the Ce $3d_{3/2}$ contributions). For $3d_{5/2}$ of Ce^{+4}, a mixing of the Ce $3d^9 4f^2 L^{n-2}$ and Ce $3d^9 4f^1 L^{n-1}$ states produces the peaks labelled v and v'', and the Ce $3d^9 4f^1 L^n$ final state forms the peak v'''. For $3d_{5/2}$ of Ce^{3+}, the Ce $3d^9 4f^2 L^{n-1}$ and Ce $3d^9 4f^1 L^n$ states correspond to peaks v and v'. For Ce $3d_{3/2}$ level with the u structure, the same assignment can be carried out.

A relationship between the area of CeO_2 in the Ce 3d spectra and the % of u''' peak (which arises from a transition of the 4f'' final state from the 4f'' initial state) was established by Shyu *et al.*[63], from which the % CeO_2 (Ce^{4+}) was calculated using the equation: % CeO_2

= % u'''/0.144. The concentration of Ce^{3+} can be also determined from the ratio: $Ce^{3+}/(Ce^{4+}+Ce^{3+})$, where Ce^{4+} and Ce^{3+} represent the sums of the integrated XPS peak areas related to Ce^{4+} (v, v'', v''', u, u'' and u''') and Ce^{3+} (v', u',) signals, respectively[29]. In Table 1 the obtained values for Ce^{3+} (%) are depicted, estimated using the equation: % Ce (III) = 100-% u'''/0.144.

Among the samples examined, the higher concentration of Ce^{3+} species (45%) is obtained by Ce-Cu-pp sample. This can be attributed to the synergistic interaction between copper and ceria, which in turn results to the facilitation of redox cycles between Cu^{2+}/Cu^{+} and Ce^{3+}/Ce^{4+}[32]. This is in agreement with the coexistence of Cu^{2+} and Cu^{+} ions in this sample, as revealed by Cu 2p XPS spectra (Figure 5).
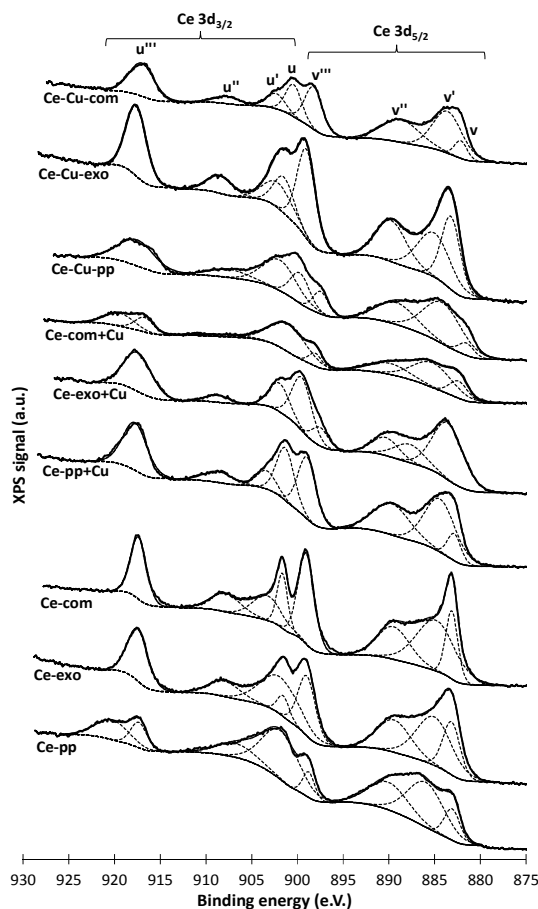
Figure 4. Ce 3d XPS results of indicated samples.

The Cu2p XPS spectra of single ceria and copper-ceria mixed oxides are depicted in Figure 5. For comparison purposes the spectra of CuO and Cu_2O commercial samples are also shown. The spectra of the samples prepared by different synthesis routes are characterized

by two main peaks of $Cu2p_{1/2}$ (approximately at 954 eV) and $Cu2p_{3/2}$ (around 934 eV), along with shake-up satellite peaks centered at ~943 eV. All samples are characterized by a Cu $2p_{3/2}$ band at ca. 934 eV, which can be attributed to fully oxidized Cu^{2+} species[29,56,68,69]. The latter is further confirmed by shake-up satellites at 944.5 eV, typically assigned to Cu^{2+} species. According to relevant literature studies, the $Cu2p_{3/2}$ at ~934 eV, in combination with the appearance of shake-up peaks are typical characteristics of CuO, while lower energies at ca. 932–933 eV and absence of shake-up peaks are characteristic of further reduced copper species, mainly Cu_2O[29,56,68-70]. The latter is confirmed in the present study by comparing the spectral features of CuO and Cu_2O samples (Figure 5). It should be noted, however, that the appearance of low intensity shake-up satellites is obvious even in the case of Cu_2O sample, implying the partial oxidation of Cu_2O sample under "measuring" conditions. This is further confirmed by the XRD analysis of the Cu_2O sample, which reveals the co-existence of CuO and Cu_2O phases.
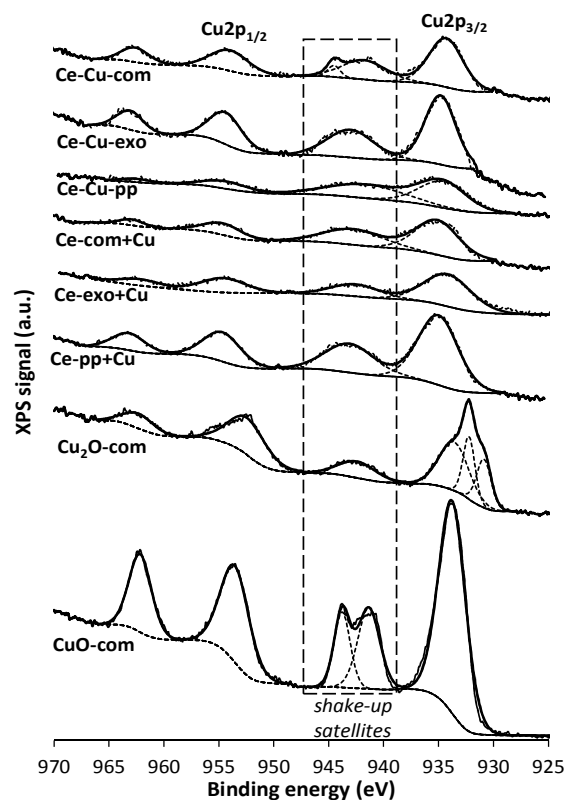
Figure 5. Cu 2p XPS results of indicated samples.

In this point, the difficulty in the unambiguous assignment of the Cu oxidation state based only on XPS results should be mentioned. Discrimination of Cu oxidation states is usually performed on the

basis of Cu2p peak position along with the evolution of Auger Cu LVV spectra; comparison of Cu2p BE and Auger parameter values in Wagner plots can provide insights toward discrimination of Cu oxidation states. Nevertheless, the great difficulty in the unambiguous assignment of the Cu state by XPS peaks position and Auger parameters has been well documented[71,72].

However, according to several comprehensive studies on XPS interpretation of Cu2p spectra[73,74], the accurate surface Cu(I)/Cu(II) ratio for samples containing both Cu(I) and Cu(II) can be obtained by estimating the ratio of the main peak/shake-up peak areas (A1/B) for a 100% pure Cu(II) sample (such as CuO). Then, the relative concentrations of Cu(I) and Cu(II) species present on the surface can be obtained by the following equations:

$$\%Cu(I)=(A-(A1/B)B)/(A+B)\times100 \qquad (1)$$

$$\%Cu(II)=B(1+(A1/B))/(A+B)\times100 \qquad (2)$$

where B is the area of the shake-up peak and A is the area of the main $Cu2p_{3/2}$ peak (Figure 5).

The qualitative analysis of pure CuO sample (Figure 5) gives an A1/B value of 1.89, in perfect agreement with the literature[73]. Based on this value the % Cu(I) in Cu-containing samples can be estimated (Table 1). It is evident that Cu-Ce mixed oxides prepared by exotemplating or precipitation, either at one stage or by subsequent incorporation of Cu into ceria, demonstrate the higher values of Cu(I) species. On the other hand, the use of commercial ceria results exclusively in Cu(II) species, independently of the preparation procedure. Among the samples examined, the highest concentration of Cu(I) species is found for Ce-Cu-pp (12%). In particular, the following order in relation to Cu(I) abundance is obtained: Ce-Cu-pp > Ce-pp+Cu > Ce-exo+Cu > Ce-Cu-exo > Ce-com+Cu ≈ Ce-Cu-com, in excellent agreement with the deN2O performance (see below). This finding implies the key role of Cu^+ species in the deN2O process, as will be discussed in the sequence.

To obtain further information regarding lattice defects and surface oxygen vacancies, micro-Raman experiments were carried out. The unpolarized Raman spectra of all samples are shown in Figure 6. All bare CeO_2 samples, prepared by different routes, present a main band at *ca.* 471cm^{-1}, which is attributed to the F_{2g} vibrational mode of the cubic fluorite-type structure of cerianite[75,76].

However, the frequency of the F_{2g} mode decreases upon Cu incorporation to the samples, following the sequence Ce-Cu-pp (448 cm^{-1}) < Ce-pp+Cu (456 cm^{-1}) < Ce-Cu-com (458 cm^{-1}) < Ce-Cu-exo (460 cm^{-1}) < Ce-exo+Cu (462 cm^{-1}) < Ce-com + Cu (468 cm^{-1}). Besides the Raman shift, the F_{2g} band becomes broader in mixed oxides Ce-Cu-pp, Ce-Cu-exo and Ce-pp+Cu, clearly revealing disorder in the system. The latter is most likely associated with the random distribution of Cu in the lattice, creating structural defects and oxygen vacancies[75,76].

More importantly, the present results match well the Cu^+/Ce^{3+} abundance (Table 1) as well as the deN2O activity sequence (see below), justifying the key role of oxygen vacancies on deN2O performance as well as their relation with the formation of Ce^{4+}/Ce^{3+} and Cu^{2+}/Cu^+ redox pairs.
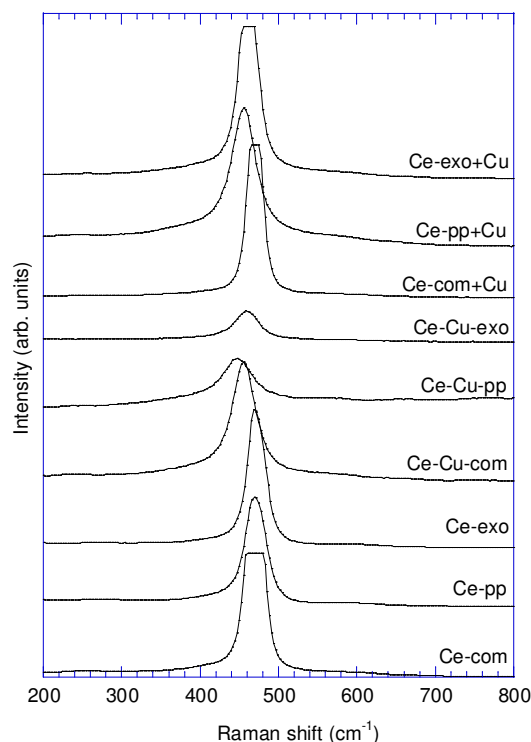
Figure 6. Raman spectra of indicated samples, recorded at room temperature, in the 200 - 800 cm^{-1} spectral range.

Catalytic activity measurements

Figure 7 depicts the deN2O performance in typical light-off experiments, in the absence of O2, over the single CeO_2 and Ce-Cu mixed oxides prepared by different routes. Significant differences among the samples are obtained, implying the strong influence of synthesis procedure on N2O decomposition. The worst behaviour is

observed for the Ce-com sample, which offers maximum N_2O conversion of about 15% at 600 ºC. Ce-exo and Ce-pp samples show better de-N_2O performance, most probably due to their improved textural characteristics, providing ~40% N_2O conversion at 600 ºC.
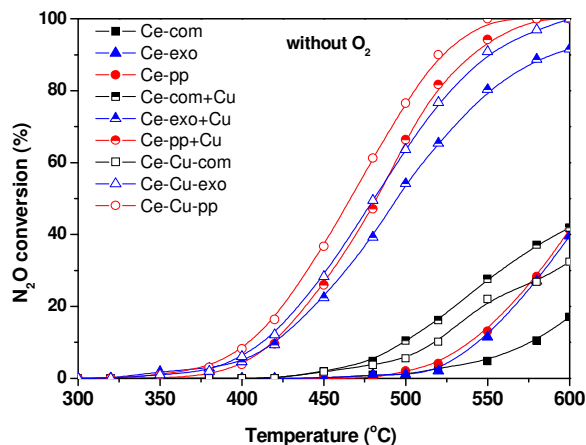
Figure 7. N_2O conversion profiles in the absence of oxygen. Reaction conditions: 1000 ppm N_2O balance He, GHSV= 40,000 h^{-1}.

Cu-Ce samples display generally better catalytic performance compared to single oxides. However, significant variations are observed amongst these samples depending on the preparation method. The samples prepared by employing commercial CeO_2 (Ce-Cu-com and Ce-com+Cu) exhibit the worst performance, similar to that obtained for single CeO_2. In contrast, very active composites can be obtained by employing Ce-pp and Ce-exo as supporting carriers. Furthermore, the preparation method which is followed for CuO incorporation into the CeO_2 (by impregnation or co-precipitation) notably affects the deN_2O performance. The optimum performance is observed for Ce-Cu-pp, prepared by co-precipitation, which achieved complete N_2O conversion at temperatures as low as 550 ºC. The following sequence, in terms of conversion performance, is recorded: Ce-Cu-pp>Ce-pp+Cu>Ce-Cu-exo>Ce-exo+Cu>Ce-com+Cu>Ce-Cu-com>Ce-pp≈Ce-exo>Ce-com. Generally, the precipitation method results in the optimum de-N_2O performance, followed by the exotemplating one. The worst behaviour is obtained for Cu-Ce samples prepared by employing commercial ceria.

The corresponding deN_2O performance under oxygen excess conditions is depicted in Figure 8. The enhanced performance under oxidizing conditions is a prerequisite for practical applications, taking into account the presence of oxygen under real exhaust conditions. In this regard, it has been reported that the activity of the most catalytic systems so far developed is drastically hindered by

adsorbed oxygen species[4,5,9]. Therefore, it is of particular importance to develop catalytic materials capable to sufficiently abate nitrous oxide emissions under oxygen excess conditions.
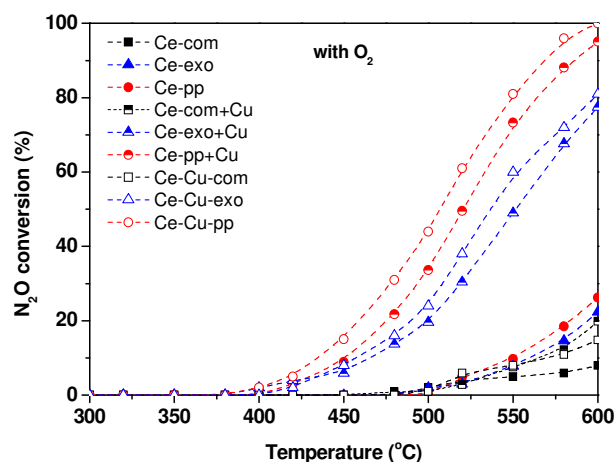
Figure 8. N_2O conversion profiles in the presence of excess oxygen. Reaction conditions: 1000 ppmv N_2O, 2.0 v/v% O_2 balance He. GHSV=40,000 h^{-1}.

By comparing the conversion profiles in the absence of oxygen (Figure 7), with those obtained in the presence of oxygen (Figure 8), some important remarks can be drawn:

i)   All catalysts are suppressed by the presence of oxygen excess.

ii)   The sequence of deN_2O performance remains unchanged both in the absence and presence of oxygen excess.

iii)   Bare CeO_2 is almost inactive under oxidizing conditions, independently of the preparation procedure.

iv)   Ce-Cu catalysts based on commercial CeO_2 are inactive, regardless the preparation technique (mechanical or impregnation).

v)   Ce-Cu catalysts prepared by exotemplating or precipitation are very active for N_2O decomposition, with the latter being more active.

vi)   The optimum performance is obtained for Ce-Cu-pp catalysts, which offers 100% N_2O conversion at ~600 ºC.

The influence of space velocity on the catalytic performance was investigated over the most effective Ce-Cu-pp catalyst. Figure 9 depicts the N_2O conversion as a function of temperature at three different values of GHSV, which are varied in the range of real exhaust systems[77], and commonly employed in several literature studies. As it can be seen the N_2O conversion profile is shifted to

slightly higher temperatures upon increasing GHSV from 10,000 to 40,000 h^{-1}. However, at temperatures higher than about 500 ºC, the Ce-Cu-pp is active enough, resulting in a complete elimination of N_2O, independently of the GHSV value utilized. This indicates that at high temperatures the decomposition rate is sufficiently high for completely remove N_2O, independently of the employed GHSV values. In contrast, at lower temperatures, where the reaction rate is slower, the residence time required for a certain N_2O conversion is higher, so, the influence of GHSV is more distinct[77].
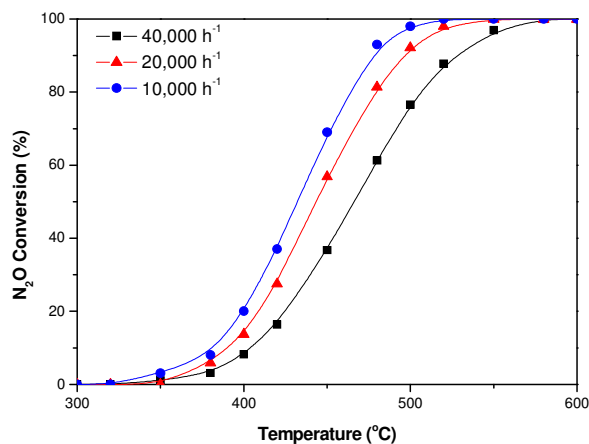
Figure 9. Effect of GHSV on N_2O conversion over Ce-Cu-pp catalysts. Reaction conditions: 1000 ppm N_2O balance He.

Long-term stability tests were finally carried out over the optimal Ce-Cu-pp materials in order to assess their potential for N_2O abatement in practical applications. Figure 10 depicts the N_2O conversion as a function of time-on-stream (TOS) at 550 ºC under oxygen excess conditions (1000 ppm N_2O + 2.0 v/v% O_2). It is obvious that the N_2O conversion remains stable at about 80% during the whole testing period (12 h). The obtained results clearly demonstrate that the Ce-Cu-pp catalysts are able to self-regenerate, through oxygen desorption from active sites even in net oxidizing conditions. However, the presence of other substances, co-existing with N_2O in real exhaust streams, such as H_2O, SO_2 and NO, should be considered in order to conclude about the practical applicability of as prepared composites. Work is in progress towards this direction.

In Table 3 the deN_2O performance of most effective Ce-Cu-pp catalysts, prepared in the present work, is compared with that of

literature reported Cu-Ce oxides and noble-metals (NMs)-based catalysts. The comparison is performed in terms of $T_{50\%}$, *i.e.,* the temperature required for 50% conversion. Although, the comparison is not straightforward due to the great variations in reaction conditions among the different research groups, a general overview can be obtained. It is evident that the half conversion temperature of Ce-Cu-pp catalysts is lower or even similar to that observed in other mixed oxides, demonstrating their superior performance. However, NMs-based catalysts, and especially Rh-based catalysts, demonstrate much lower T_{50} temperatures, due to the excellent intrinsic characteristics of Rh. The lower cost of mixed oxides compared to particularly expensive NMs, could however counterbalance their inferior performance.
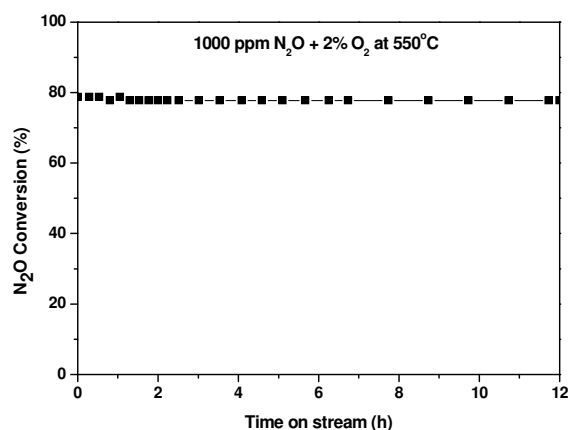
Figure 10. N_2O conversion as a function of time on stream (12 h) at 550 ºC, in the presence of excess oxygen. Reaction conditions: 1000 ppm N_2O, 2.0 v/v% O_2 balance He. GHSV=40,000 h^{-1}.

On the light of the above results, it can be noticed that the preparation procedure notably affects the N_2O decomposition performance of CuO-CeO_2 mixed oxides. It was clearly revealed that all Cu-Ce mixed oxides prepared at one stage, demonstrated better deN_2O performance compared to the corresponding ones prepared by Cu incorporation to ceria *via* impregnation. Furthermore the superiority of CuO-CeO_2 mixed oxides prepared by co-precipitation, compared to those obtained by impregnation or exo-templating was clearly revealed.

Table 3. N_2O conversion performance of prepared samples in comparison to that reported in literature.

Catalyst	Reaction conditions	T_{50} (°C)	Ref.
0.5 wt.% Rh/Al₂O₃	0.1% N_2O; GHSV=10,000 h^{-1}	340	[78]
0.5 wt.% Rh/CeO₂	0.1% N_2O; GHSV=10,000 h^{-1}	275	[78]
0.5 wt.% Pd/Al₂O₃	0.1% N_2O; GHSV=10,000 h^{-1}	>500	[78]
0.5 wt.% Pd/CeO₂	0.1% N_2O; GHSV=10,000 h^{-1}	475	[78]
0.5 wt.% Pt/Al₂O₃	0.1% N_2O; GHSV=10,000 h^{-1}	500	[78]
0.5 wt.% Pt/CeO₂	0.1% N_2O; GHSV=10,000 h^{-1}	465	[78]
2.0 wt.% Rh/Al₂O₃	0.095% N_2O; WHSV=60,000 cm^3 g^{-1} h^{-1}	240	[79]
5 wt.% Ru/MCM-41	10% N_2O; GHSV=4,000 h^{-1}	360	[80]
2 wt.% Rh/Al₂O₃	0.05% N_2O; WHSV=30,000 cm^3 g^{-1} h^{-1}	350	[81]
67 mol% Cu/CeO₂	0.26% N_2O; GHSV=19,000 h^{-1}	370	[26]
35.5 mol% Cu/CeO₂	0.25% N_2O; GHSV=45,000 h^{-1}	440	[27]
5 mol% Cu/CeO₂	5.0 % N_2O; WHSV= 5,100 cm^3 g^{-1} h^{-1}	430	[25]
10 wt.% Cu/CeO₂	0.25% N_2O; WHSV= 60,000 cm^3 g^{-1} h^{-1}	380	[24]
20 wt.% Cu/CeO₂ *40 mol% Cu (CeO₂ balance)*	0.10 % N_2O; GHSV=40,000 h^{-1}	465	This work
20 wt.% Cu/CeO₂ *40 mol% Cu (CeO₂ balance)*	0.10 % N_2O; GHSV=10,000 h^{-1}	430	This work

Taking into account the results of physicochemical and surface characterizations, Ce-Cu-pp samples display the optimum redox properties in terms of reducibility (Figure 2) and Cu^+/Ce^{3+} species population (Table 1). These factors can be considered crucial for N_2O decomposition, given the redox mechanism of N_2O decomposition. More specifically, N_2O decomposition mechanism involves molecular adsorption of N_2O, followed subsequently by N-O bond scission and N_2 desorption[82]. In this particular type of mechanism the re-combination of neighbouring oxygen species toward molecular oxygen desorption and active sites regeneration, is of major importance for N_2O adsorption and consequent dissociation.

In relation to CuO-CeO_2 catalysts, the following reaction mechanism can be proposed:

$$Cu^+ + N_2O \rightarrow Cu^+\text{-}ONN \qquad (3)$$

$$Cu^+\text{-}ONN \rightarrow Cu^{+2}\text{-}O^- + N_2 \qquad (4)$$

$$Cu^{2+}\text{-}O^- + Cu^{2+}\text{-}O^- \rightarrow 2Cu^+ + O_2 \qquad (5)$$
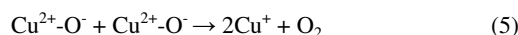
However in the case of isolated $Cu^{2+}\text{-}O^-$ sites the recombination of oxygen species towards molecular oxygen desorption is notably hindered[24]. For that reason, the regeneration of active sites through mobile oxygen species derived from CeO_2 could be also considered[24]:

$$Cu^{2+}\text{-}O^- + Ce^{3+} \rightarrow Cu^+ + Ce^{4+}\text{-}O^- \qquad (6)$$

$$2Ce^{4+}\text{-}O^- \rightarrow 2Ce^{3+} + O_2 \qquad (7)$$

The superior deN$_2$O performance of Ce-Cu-pp catalyst can be more thoroughly interpreted by taking into account the electronic metal support interaction (EMSI) effect, described previously. Based on the obtained results, it is evident that the Ce-Cu-pp catalyst demonstrated optimum reducibility, in terms of H$_2$-TPR temperature, due to metal-support interactions. Moreover, the relative abundance of Cu$^+$ and Ce^{3+} species in Ce-Cu-pp samples points to the synergistic interactions between copper and ceria, which in turn facilitate the redox cycles between Cu^{2+}/Cu$^+$ and Ce^{3+}/Ce^{4+} pairs.

In particular, the modification of copper surface/redox properties could be considered as a consequence of perturbations in the electronic properties, originating from bonding interactions with ceria[83]. In a similar manner, it has been demonstrated that the strong interaction between Ni nanoparticles and ceria produces large electronic perturbations, with significant impact on the catalytic performance. More importantly, the alteration of the Ce^{3+}/Ce^{4+} ratio in the CeO$_2$ carrier results in a notable modification of the redox/surface properties of Ni particles, illustrating the key role of electronic metal–support interactions[83]. The stabilization of Cu$^+$ clusters by cerium oxide, and, in turn, the increased active oxygen on cerium *via* the redox equilibrium Cu^{2+} + Ce^{3+} ↔ Cu$^+$ + Ce^{4+} has been already invoked to explain the high oxidation activity of Cu/CeO$_2$ catalysts[84,85]. The lowering of the redox potential of Cu species in the CeO$_2$ matrix *via* the electronic interaction between Ce4f, O2p and Cu3d orbitals, has been also proposed[86]:

$$Ce^{4+}\text{–}O^{2\text{-}}\text{–}Cu^{2+} + e^- \leftrightarrow Ce^{4+}\text{–}O^{2\text{-}}\text{–}Cu^+ \leftrightarrow Ce^{3+}\text{–}O^{2\text{-}}\text{–}Cu^{2+} \leftrightarrow Ce^{4+}\text{–}O^{2\text{--}}Cu^{2+} + e^-$$
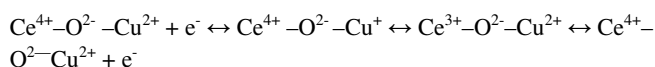
Consequently, the better performance of Ce-Cu-pp samples can be ascribed to their superior reducibility at low temperatures in conjunction with the high concentration of Cu$^+$/Ce^{3+} sites. These factors are crucial for N$_2$O decomposition, since they contribute to the facilitation of oxygen ad-atoms desorption from the catalyst surface (reactions (5) and (7)) as well as to the regeneration of active sites (reaction (6)). The crucial role of the Ce^{3+}/Ce^{4+} redox pair in the de-N$_2$O process has been already mentioned in Rh/CeO$_2$[87] and Cu-Ce mixed oxides[24,26,88].

Conclusions

The N$_2$O decomposition over bare or mixed CeO$_2$ and CuO oxides was investigated in the present study, with particular emphasis on the impact of synthesis procedure (impregnation, precipitation, exo-

templating) on the surface and redox properties. The results clearly revealed that Ce-Cu samples display better catalytic performance compared to single oxides, which however depends notably on the preparation method. The optimum performance is observed for Ce-Cu mixed oxides, prepared by co-precipitation, which achieved complete N$_2$O conversion at temperatures as low as 550 ºC. Moreover, these samples demonstrated excellent stability and tolerance toward excess oxygen presence. The results are mainly interpreted on the basis of characterization studies, which revealed that significant modifications on the surface and redox properties of catalysts can be induced by the synthesis procedure. The superiority of Ce-Cu mixed oxides prepared by precipitation can be ascribed to their excellent reducibility as well as to the facilitation of Ce^{4+}/Ce^{3+} and Cu^{2+}/Cu$^+$ redox cycles. A redox mechanism of N$_2$O decomposition was proposed involving N$_2$O adsorption on Cu$^+$ sites and their subsequent regeneration through Cu-ceria interactions.

References

[1]   http://epa.gov/climatechange/ghgemissions/gases/n2o.html, accessed 14.11.2014.

[2]   S. Rao, K. Riahi, The role of non-CO$_2$ greenhouse gases in climate change mitigation: Long-term scenarios for the 21st century, *Energy J.*, 2006, **27**, 177.

[3]   A. R. Ravishankara, J. S. Daniel, R. W. Portmann, Nitrous oxide (N$_2$O): The dominant ozone-depleting substance emitted in the 21st century, *Science,* 2009, **326**, 123.

[4]   J. Perez-Ramirez, F. Kapteijn, K. Schoffel, J.A. Moulijn, Formation and control of N$_2$O in nitric acid production. Where do we stand today, *Appl. Catal. B,* 2003, **44**, 117.

[5]   J. Perez-Ramirez, Prospects of N$_2$O emission regulations in the European fertilizer industry, Appl. Catal. B, 2007, **70**, 31.

[6] M. Galle, D.W. Agar, O. Watzenberger, Thermal N_2O decomposition in regenerative heat exchanger reactors, *Chem. Eng. Sci.*, 2001, **56**, 1587.

[7] G. Centi, F. Vazzana, Selective catalytic reduction of N_2O in industrial emissions containing O_2, H_2O and SO_2: behavior of Fe/ZSM-5 catalysts, *Catal. Today*, 1999, **53**, 683.

[8] S. Kameoka, K. Kita, T. Takeda, S. Tanaka, S. Ito, K. Yuzaki, T. Miyadera, K. Kunimori, Simultaneous removal of N_2O and CH_4 as the strong greenhouse-effect gases over Fe-BEA zeolite in the presence of excess O_2, *Catal. Lett.*, 2000, **69**, 169.

[9] F. Kapteijn, J. Rodriguez-Mirasol, J.A. Moulijn, Heterogeneous catalytic decomposition of nitrous oxide, *Appl. Catal. B*, 1996, **9**, 25.

[10] A. Dandekar, M.A. Vannice, Decomposition and reduction of N_2O over copper catalysts, *Appl. Catal. B*, 1999, **22**, 179.

[11] J. Perez-Ramirez, J. Overeijnder, F. Kapteijn, J.A. Moulijn, Structural promotion and stabilizing effect of Mg in the catalytic decomposition of nitrous oxide over calcined hydrotalcite-like compounds, *Appl. Catal. B*, 1999, **23**, 59.

[12] X.D. Xu, H.L. Xu, F. Kapteijn, J.A. Moulijn, SBA-15 based catalysts in catalytic N_2O decomposition in a model tail-gas from nitric acid plants, *Appl. Catal. B*, 2004, **53**, 265.

[13] A.C. Gluhoi, M.A.P. Dekkers, B.E. Nieuwenhuys, Comparative studies of the N_2O/H_2, N_2O/CO, H_2/O_2 and CO/O_2 reactions on supported gold catalysts: effect of the addition of various oxides, *J. Catal.*, 2003, **219**, 197-205.

[14] A.C. Gluhoi, S.D. Lin, B.E. Nieuwenhuys, The beneficial effect of the addition of base metal oxides to gold catalysts on reactions relevant to air pollution abatement, *Catal. Today*, 2004, **90**, 175-181.

[15] X. Zhang, Q. Shen, C. He, C. Ma, J. Cheng, Z. Liu and Z. Hao, Decomposition of nitrous oxide over Co-zeolite catalysts: role of zeolite structure and active site, *Catal. Sci. Technol.*, 2012, **2**, 1249.

[16] X. Zhang, Q. Shen, C. He, C. Ma, J. Cheng and Z. Hao, Investigation of nitrous oxide decomposition over highly active and stable bimetallic CoFe-MOR zeolite catalyst: effective removal and mechanism study, *Catal. Sci. Technol.*, 2012, **2**, 1059.

[17] A. Ates, Influence of treatment conditions on decomposition activity of N_2O over FeZSM-5 with high iron content, *Catal. Sci. Technol.*, 2014, **4**, 2031.

[18] R. Amrousse, Po-Jul Chang, A. Choklati, A. Friche, M. Rai, A. Bachar, C. Follet-Houttemane and K. Hori, Catalytic decomposition of N_2O over Ni and Mg-magnetite catalysts, *Catal. Sci. Technol.*, 2013, **3**, 2288.

[19] B. Ul-ain, A. Zafar and S. Ahmed, To explore a new class of material (X-type hexaferrites) for N_2O decomposition, *Catal. Sci. Technol.*, 2015, **5**, 1076.

[20] F.J. Perez-Alonso, I. Melian-Cabrera, M.L. Granados, F. Kapteijn, J.L.G. Fierro, Synergy of $Fe_xCe_{1-x}O_2$ mixed oxides for N_2O decomposition, *J. Catal.*, 2006, **239**, 340.

[21] L. Xue, C.B. Zhang, H. He, Y. Teraoka, Catalytic decomposition of N_2O over CeO_2 promoted Co_3O_4 spinel catalyst, *Appl. Catal. B*, 2007, **75**, 167.

[22] A. Trovarelli, Catalysis by Ceria and Related Materials, *Imperial College Press*, London, 2002, 508.

[23] B.M. Abu-Zied, S.A. Soliman, S.E. Abdellah, Enhanced direct N_2O decomposition over $Cu_xCo_{1-x}Co_2O_4$ ($0.0 \leq x \leq 1.0$) spinel-oxide catalysts, *J. Ind. Eng. Chem.*, 2015, **21**, 814.

[24] M. Zabilskiy, P. Djinovic, B. Erjavec, G. Drazic, A. Pintar, Small CuO clusters on CeO_2 nanospheres as active species for catalytic N_2O decomposition, *Appl. Catal. B*, 2015, **163**, 113.

[25] A. Adamski, W. Zajac, F. Zasada, Z. Sojka, Copper ionic pairs as possible active sites in N_2O decomposition on CuO_x/CeO_2 catalysts, *Catal. Today*, 2012, **191**, 129.

[26] H. Zhou, Z. Huang, C. Sun, F. Qin, D. Xiong, W. Shen, H. Xu, Catalytic decomposition of N_2O over $Cu_xCe_{1-x}O_y$ mixed oxides, *Appl. Catal. B*, 2012, **125**, 492.

[27] M. Zabilskiy, B. Erjavec, P. Djinovic, A. Pintar, Ordered mesoporous $CuO–CeO_2$ mixed oxides as an effective catalyst for N_2O decomposition, *Chem. Eng. J.*, 2014, **254**, 153.

[28] M. Konsolakis, Z. Ioakeimidis, Surface/structure functionalization of copper-based catalysts by metal-support and/or metal–metal interactions, *Appl. Surf. Sci.*, 2014, **320**, 244.

[29] M. Konsolakis, S.A.C. Carabineiro, P.B. Tavares, J.L. Figueiredo, Redox properties and VOC oxidation activity of Cu catalysts supported on $Ce_{1-x}Sm_xO_\delta$ mixed oxides, *J. Haz. Mater.*, 2013, **261**, 512.

[30] X. Wang, J.A. Rodriguez, J.C. Hanson, D. Gamarra, A. Martinez Arias, M. Fernàndez-García, In Situ Studies of the Active Sites for the Water Gas Shift Reaction over $Cu–CeO_2$ Catalysts: Complex Interaction between Metallic Copper and Oxygen Vacancies of Ceria, *J. Phys. Chem. B*, 2006, **110**, 428.

[31] M.F. Luo, J.M. Ma, J.Q. Lu, Y.P. Song, Y.J. Wang, In Situ Studies of the Active Sites for the Water Gas Shift Reaction over

Cu–CeO$_2$ Catalysts: Complex Interaction between Metallic Copper and Oxygen Vacancies of Ceria, *J. Catal.,* 2007, **246**, 52.

[32]   S.Y. Wang, N. Li, L.F. Luo, W.X. Huang, Z.Y. Pu, Y.J. Wang, G.S. Hu, M.F. Luo, J.Q. Lu, Probing different effects of surface MO$_y$ and Mn$^+$ species (M = Cu, Ni, Co, Fe) for xMO$_y$/Ce$_{0.9}$M$_{0.1-x}$O$_{2-\delta}$ catalysts in CO oxidation, *Appl. Catal. B,* 2014, **144**, 325-332.

[33]   X. Li, X.-Y. Quek, D.A.J. Michel Ligthartb, M. Guoa, Y. Zhang, C. Li, Q. Yanga, E.J.M. Hensen, CO–PROX reactions on copper cerium oxide catalysts prepared by melt infiltration, *Appl. Catal. B,* 2012, **123-124**, 424.

[34]   A. Al-Musa, M. Al-Saleh, Z.C. Ioakeimidis, M. Ouzounidou, I.V. Yentekakis, M. Konsolakis, G.E. Marnellos, Hydrogen production by iso-octane steam reforming over Cu catalysts supported on rare earth oxides (REOs), *Int. J. Hydrogen Energy,* 2014, **39**, 1350.

[35]   A.P. Jia, G.S. Hu, L. Meng, Y.L. Xie, J.Q. Lu, M.F. Luo, CO oxidation over CuO/Ce$_{1-x}$Cu$_x$O$_{2-\delta}$ and Ce$_{1-x}$Cu$_x$O$_{2-\delta}$ catalysts: Synergetic effects and kinetic study, *J. Catal.,* 2012, **289**, 199.

[36]   F. Lin, X. Wu, D. Weng, Effect of barium loading on CuOx–CeO$_2$ catalysts: NOx storage capacity, NO oxidation ability and soot oxidation activity, *Catal. Today,* 2011, **175**, 124.

[37]   A. Martinez-Arias, M. Fernàndez-García, J. Soria, J.C. Conesa, Spectroscopic study of a Cu/CeO$_2$ catalyst subjected to redox treatments in carbon monoxide and oxygen, *J. Catal.,* 1999, **182**, 367.

[38]   A. Martinez-Arias, A.B. Hungria, M. Fernàndez-García, J.C. Conesa, G. Munuera, Interfacial Redox Processes under CO/O$_2$ in a Nanoceria-Supported Copper Oxide Catalyst, *J. Phys. Chem. B,* 2004, **108**, 17983.

[39]   A. Martinez-Arias, D. Gamarra, M. Fernàndez-García, X.Q. Wang, J.C. Hanson, J.A. Rodriguez, Comparative study on redox properties of nanosized CeO$_2$ and CuO/CeO$_2$ under CO/O$_2$, *J. Catal.,* 2006, **240**, 1.

[40]   A. Martinez-Arias, D. Gamarra, M. Fernàndez-García, A. Hornes, P. Bera, Z. J.A. Koppany, Z. Schay, Redox-catalytic correlations in oxidised copper-ceria CO-PROX catalysts, *Catal. Today,* 2009, **143**, 211.

[41]   S.S.T. Bastos, J.J.M. Órfão, M.M.A. Freitas, M.F.R. Pereira, J.L. Figueiredo, Manganese oxide catalysts synthesized by exotemplating for the total oxidation of ethanol, *Appl. Catal. B,* 2009, **93**, 30.

[42]   S.S.T. Bastos, S.A.C. Carabineiro, J.J.M. Órfão, M.F.R. Pereira, J.J. Delgado, J.L. Figueiredo, Total oxidation of ethyl acetate, ethanol and toluene catalyzed by exotemplated manganese and cerium oxides loaded with gold, *Catal. Today,* 2012, **180**, 148.

[43]   M. Schwickardi, T. Johann, W. Schmidt, F. Schüth, High-surface-area oxides obtained by an activated carbon route, *Chem. Mater.,* 2002, **14**, 3913.

[44]   S.A.C. Carabineiro, S.S.T. Bastos, J.J.M. Órfão, M.F.R. Pereira, J.J. Delgado, J.L. Figueiredo, Carbon monoxide oxidation catalysed by exotemplated manganese oxides, *Catal. Lett.,* 2010, **134**, 217.

[45]   S.A.C. Carabineiro, S.S.T. Bastos, J.J.M. Órfão, M.F.R. Pereira, J.J. Delgado, J.L. Figueiredo, Exotemplated ceria catalysts with gold for CO oxidation, *Appl. Catal. A,* 2010, **381**, 150.

[46]   X. Chen, S.A.C. Carabineiro, S.S.T. Bastos, P.B. Tavares, J.J.M. Órfão, M.F.R. Pereira, J.L. Figueiredo, Exotemplated copper, cobalt, iron, lanthanum and nickel oxides for catalytic oxidation of ethyl acetate, *J. Environ. Chem. Eng.,* 2013, **1**, 795.

[47]   X. Chen, S.A.C. Carabineiro, S.S.T. Bastos, P.B. Tavares, J.J.M. Órfão, M.F.R. Pereira, J.L. Figueiredo, Catalytic oxidation of ethyl acetate on cerium-containing mixed oxides, *Appl. Catal. A,* 2014, **472**, 101.

[48]   X. Chen, S.A.C. Carabineiro, P.B. Tavares, J.J.M. Órfão, M.F.R. Pereira, J.L. Figueiredo, Catalytic oxidation of ethyl acetate over La-Co and La-Cu oxides, *J. Environ. Chem. Eng.,* 2014, **2**, 344.

[49]   S.A.C. Carabineiro, X. Chen, M. Konsolakis, A.C. Psarras, P.B. Tavares, J.J.M. Órfão, M.F.R. Pereira, J.L. Figueiredo, Catalytic oxidation of toluene on Ce-Co and La-Co mixed oxides synthesized by exotemplating and evaporation methods, *Catal. Today,* 2015, **244**, 161.

[50]   N. Job, R. Pirard, J. Marien, J.-P. Pirard, Porous carbon xerogels with texture tailored by pH control during sol–gel process, *Carbon,* 2004, **42**, 619.

[51]   S.A.C. Carabineiro, T. Thavorn-amornsri, M.F.R. Pereira, J.L. Figueiredo, Adsorption of ciprofloxacin on surface modified carbon materials, *Water Res.,* 2011, **45**, 4583.

[52]   S.A.C. Carabineiro, T. Thavorn-amornsri, M.F.R. Pereira, P. Serp, J.L. Figueiredo, Comparison between activated carbon, carbon xerogel and carbon nanotubes for the adsorption of the antibiotic ciprofloxacin, *Catal. Today,* 2012, **186**, 29.

[53]   S.A.C. Carabineiro, L.M.D.R.S. Martins, J.G. Buijnsters, M. Avalos-Borja, A.J.L. Pombeiro, J.L. Figueiredo, Gold nanoparticles

supported on carbon materials for cyclohexane oxidation, *Appl. Catal. A,* 2013, **467**, 279.

[54]   F. Schüth, Endo- and exotemplating to create high-surface-area inorganic materials, *Angew. Chem. Int. Ed.,* 2003, **42**, 3604.

[55]   J. Wang, P.A. Chernavskii, A.Y. Khodakov, Y. Wang, Structure and catalytic performance of alumina-supported copper–cobalt catalysts for carbon monoxide hydrogenation, *J. Catal.,* 2012, **286**, 51.

[56]   L. Kundakovic, M. Flytzani-Stephanopoulos, Reduction characteristics of copper oxide in cerium and zirconium oxide systems, *Appl. Catal. A,* 1998, **171**, 13.

[57]   S. Brunauer, P.H. Emmett, E. Teller, Adsorption of gases in multimolecular layers, *J. Am. Chem. Soc.,* 1938, 60, 309.

[58]   S.A.C. Carabineiro, N. Bogdanchikova, M. Avalos-Borja, A. Pestryakov, P.B. Tavares, J.L. Figueiredo, Gold supported on metal oxides for carbon monoxide oxidation, *NanoRes.,* 2011, **4**, 180.

[59]   M.-F. Luo, J.-M. Ma, J.-Q. Lu, Y.-P. Song, Y.-J. Wang, High-surface area CuO–CeO2 catalysts prepared by a surfactant-templated method for low-temperature CO oxidation, *J. Catal.,* 2007, **246**, 52.

[60]   N. Acerbi, S.C.E. Tsang, G. Jones, S. Golunski, P.Collier, Rationalization of Interactions in Precious Metal/Ceria Catalysts Using the d-Band Center Model,, *Angew. Chem. Int. Ed.*, 2013, **52**, 7737.

[61]   N. Acerbi, S. C. Tsang, S. Golunski, P. Collier, A practical demonstration of electronic promotion in the reduction of ceria coated PGM catalysts, *Chem. Commun.*, 2008, 1578.

[62]   J. Frost, Junction effect interactions in methanol synthesis catalysts, *Nature*, 1988, **334**, 577.

[63]   J.Z. Shyu, K. Otto, W.L.H. Watkins, G.W. Graham, R.K. Belitz, H.S. Gandhi, Characterization of Pd/γ-alumina catalysts containing ceria, *J. Catal.,* 1988, **114**, 23.

[64]   S. Tsunekawa, T. Fukuda, A. Kasuya, X-ray photoelectron spectroscopy of monodisperse CeO_{2-x} nanoparticles, *Surf. Sci.,* 2000, 457, L437.

[65]   C. Sun, H. Li, L. Chen, Study of flowerlike CeO_2 microspheres used as catalyst supports for CO oxidation reaction, *J. Phys. Chem. Solids,* 2007, **68**, 1785.

[66]   C. Pan, D. Zhang, L. Shi, J. Fang, Template-Free Synthesis, Controlled Conversion, and CO Oxidation Properties of CeO_2 Nanorods, Nanotubes, Nanowires, and Nanocubes, *Eur. J. Inorg. Chem.,* 2008, 2429.

[67]   V. Matolín, I. Matolínová, L. Sedláček, K.C. Prince, T. Skála, A resonant photoemission applied to cerium oxide based nanocrystals, *Nanotechnology,* 2009, **20**, 215706.

[68]   W. Li, M. Flytzani-Stephanopoulos, Total oxidation of carbon-monoxide andmethane over transition metal fluorite oxide composite catalysts: II. Catalyst characterization and reaction-kinetics, *J. Catal.,* 1995, **153**, 317.

[69]   J.L. Ayastuy, A. Gurbani, M.P. González-Marcos, M.A. Gutiérrez-Ortiz, Selective CO oxidation in H_2 streams on $CuO/Ce_xZr_{1-x}O_2$ catalysts: correlation between activity and low temperature reducibility, *Int. J. Hydrogen Energy,* 2012, **37**, 1993.

[70]   C. Lamonier, A. Bennani, A. D' Huysser, A. Aboukaïs, G. Wrobel, Evidence for different copper species in precursors of copper–cerium oxide catalysts for hydrogenation reactions. An X-ray diffraction, EPR and X-ray photoelectron spectroscopy study, *J. Chem. Soc. Faraday Trans.,* 1996, **92**, 131.

[71]   J. Gimenez-Manogil, A. Bueno-Lopez, A. García- García, Preparation, characterisation and testing of $CuO/Ce_{0.8}Zr_{0.2}O_2$ catalysts for NO oxidation to NO_2 and mild temperature diesel soot combustion, *Appl. Catal. B,* 2014, **152-153**, 99.

[72]   J.P. Espinos, J. Morales, A. Barranco, A. Caballero, J.P. Holgado, A.R. GonzalezElipe, Interface Effects for Cu, CuO, and Cu_2O Deposited on SiO_2 and ZrO_2. XPS Determination of the Valence State of Copper in Cu/SiO_2 and Cu/ZrO_2 Catalysts, *J. Phys. Chem.,* 2002, **106**, 6921.

[73]   M.C. Biesinger, L.W.M. Lau, A.R. Gerson, R.St.C. Smart, Resolving surface chemical states in XPS analysis of first row transition metals, oxides and hydroxides: Sc, Ti, V, Cu and Zn, *Appl. Surf. Sci.*, 2010, **257**, 887.

[74]   M.C. Biesinger, B.R. Hart, R. Polack, B.A. Kobe, R.St.C. Smart, Analysis of mineral surface chemistry in flotation separation using imaging XPS, *Minerals Eng.*, 2007, **20**, 152.

[75]   L. Qi, Q. Yu, Y. Dai, C. Tang, L. Liu, H. Zhang, F. Gao, L. Donga, Y. Chena, Influence of cerium precursors on the structure and reducibility of mesoporous $CuO-CeO_2$ catalysts for CO oxidation, *Appl. Catal. B: Environ.*, 2012, **119–120**, 308.

[76]   A. Gurbani, J.L. Ayastuy, M.P. González-Marcos, M.A. Gutiérrez-Ortiz, $CuO-CeO_2$ catalysts synthesized by various methods: Comparative study of redox properties, *Int. J. Hydrogen Energ,.* 2010, **35**, 11582.

[77]   E. Ruiz-Martínez, J.M. Sánchez-Hervás, J. Otero-Ruiz, Effect of operating conditions on the reduction of nitrous oxide by propane over a Fe-zeolite monolith, *Appl. Catal. B,* 2005, **61**, 306.

[78] S. Parres-Esclapez, M.J. Illan-Gomez, C. Salinas-Martinez de Lecea, A. Bueno-Lopez, On the importance of the catalyst redox properties in the N_2O decomposition over alumina and ceria supported Rh, Pd and Pt, *Appl. Catal. B,* 2010, **96**, 370.

[79] K. Yuzaki, T. Yarimizu, S.-I. Ito, K.K. Kunimori. Catalytic decomposition of N_2O over supported rhodium catalysts: high activities of Rh/USY and Rh/Al_2O_3 and the effect of Rh precursors, *Catal. Lett.,* 1997, **47**, 173.

[80] S. Kawi, S.Y. Liu, S.-C. Shen, Catalytic decomposition and reduction of N_2O on Ru/MCM-41 catalyst, *Catal. Today*, 2001, **68,** 237.

[81] S.C. Christoforou, E.A. Efthimiadis, I.A. Vasalos, Catalytic Conversion of N_2O to N_2 over Metal-Based Catalysts in the Presence of Hydrocarbons and Oxygen, *Catal. Lett.,* 2002, **79**, 137.

[82] W.B. Tolman, Binding and Activation of N_2O at Transition Metal Centers: Recent Mechanistic Insights, *Angew. Chem. Ind. Ed.,* 2010, **49**, 1018.

[83] S.D. Senanayake, J.A. Rodriguez, D. Stacchiola, Electronic Metal–Support Interactions and the Production of Hydrogen Through the Water-Gas Shift Reaction and Ethanol Steam Reforming: Fundamental Studies with Well-Defined Model Catalysts, *Top. Catal.*, 2013, **56**, 1488.

[84] W. Liu, M. Flytzani-Stephanopoulos, Transition metal-promoted oxidation catalysis by fluorite oxides: A study of CO oxidation over $Cu-CeO_2$, *Chem. Eng. J.*, 1996, **64**, 283.

[85] L. Qi, Q. Yu, Y. Dai, C. Tang, L. Liu, H. Zhang, F. Gao, L. Dong, Y. Chen, Influence of cerium precursors on the structure and reducibility of mesoporous $CuO-CeO_2$ catalysts for CO oxidation, *Appl. Catal. B*, 2012, **119-120**, 308.

[86] P. Bera M.S. Hegde, S. Mitra, S. Sampath, Promoting effect of CeO_2 in a Cu/CeO_2 catalyst: lowering of redox potentials of Cu species in the CeO_2 matrix, *Chem. Commun.*, 2001, 927.

[87] S. Parres-Esclapez, M.J. Illan-Gomez, C. Salinas-Martinez de Lecea, A. Bueno Lopez, Preparation and characterisation of γ-Al_2O_3 particles-supported $Rh/Ce_{0.9}Pr_{0.1}O_2$ catalyst for N_2O decomposition in the presence of O_2, H_2O and NO, *Int. J. Greenh. Gas Control,* 2012, **11**, 251.

[88] J. Ma, N.M. Rodriguez, M.A. Vannice, R.T.K. Baker, Nitrous oxide decomposition and reduction over copper catalysts supported on various types of carbonaceous materials, *Top. Catal.,* 2000, **10**, 27.